Measuring conditions for second order X-ray Bragg-spectrometry

To cite this article: J Dellith *et al* 2014 *IOP Conf. Ser.: Mater. Sci. Eng.* **55** 012003

IOP Conf. Series: Materials Science and Engineering **55** (2014) 012003 doi:10.1088/1757-899X/55/1/012003

Measuring conditions for second order X-ray Bragg-spectrometry

J Dellith, A Scheffel and M Wendt

Institute of Photonic Technology, Albert-Einstein-Strasse 9, DE-07745 Jena, Germany

E-mail: jan.dellith@ipht-jena.de

Abstract. The $KL_{2,3}$ $(\alpha)_{1,2}$-lines of ^{19}K, the $L_3M_{4,5}$ $(\alpha)_{1,2}$-lines of ^{48}Cd, and the $M_5N_{6,7}$ $(\alpha)_{1,2}$-lines of ^{92}U are lines of comparable energy in the region of approximately 3 keV. In none of these cases were we able to resolve the three doublets when recording the spectra in first order Bragg spectrometry using a PET crystal as the dispersing element. For the purpose of enhancing the resolving power of the spectrometer, the three α spectra were recorded in second order reflection, thereby transferring the lines into another spectral region dominated by X-ray quanta of half the energy. In order to achieve high net peak intensities as well as a high peak-to-background ratio and, consequently, a high level of detection capability, the discriminator settings should be optimized quite carefully. In this manner, we were able to resolve the three α doublets and estimate α_2/α_1 intensity ratios. Inexplicably, current monographs, e.g., by Goldstein *et al*, do not contain any indications about the rational use of high order spectrometry. Only a few rather old monographs contain some hints in this regard.

1. Introduction

Compared to energy-dispersive X-ray spectrometry (EDS), wavelength-dispersive X-ray spectrometry (WDS) provides a better energy resolution and, consequently, a higher sensitivity for the detection of trace elements. However, WDS measurements are more time-consuming and also more complicated than EDS measurements because the measured WD intensities depend on a number of circumstances which can be neglected in ED measurements. For example, EDS spectra are completely free of influences caused by high order reflections. Most of the aspects described in connection with high order reflections focus on their disturbing effects. Here, the interference possibility of a given characteristic X-ray line with one originating from high order reflections is discussed initially. In fact, this aspect is problematic, particularly in the field of light element analysis, because often only one usable X-ray line is available. To give an example: In the analysis of boron doped silica, the boron KL_3 (α)-line at 183 eV interferes with the third order reflection of the oxygen KL_3 (α)-line with an energy of 525 eV. Normally, the high order reflections can be efficiently discriminated by using the pulse height analysis mode. However, especially in the example mentioned above, it is sometimes tricky because of the spread pulse height spectrum of the soft boron K-radiation [1].

On the other hand, there are quite useful applications of high order reflections. For instance, a precise calibration of wavelength-dispersive X-ray spectrometers can be achieved using one and the same element and measuring the spectra in first, second, and third order reflection. Furthermore, in the simultaneous quantitative analysis of trace and major elements, the strong line intensities and subsequent high count rates of the major elements can be reduced by falling back on high order spectra, the intensity of which is only a fraction of those of the first order. But perhaps the most

important reason for using high order reflections is the possibility of improving the resolving power of a given WD spectrometer and consequently enhancing the line separation.

Unfortunately, information about useful aspects of high order WD spectrometry can only be found in a few rather old specialized books, e.g., by Müller [2] or Jenkins [3]. In the current monographs by Reed [4], Scott *et al* [5], or Goldstein *et al* [6] this topic is completely lacking.

In two previous works, we studied the M-spectra of ^{68}Er [7] and ^{92}U [8], and have already briefly reported on the potential of high order spectrometry. In the present work, we aim to illustrate the resolution enhancement in particular. We will propose a strategy to determine optimized discriminator settings, which are a basic requirement to achieving high peak-to-background ratios and a level of detection capability which is comparable to that provided by first order spectrometry.

2. Experimental method

The measurements were carried out using a JEOL JXA-8800L microprobe analyzer (Jeol Ltd., Tokyo, Japan). The take-off angle of this instrument is 40°. All spectra were recorded using a PET crystal with a periodicity of 2d = 8.742 Å as the dispersing element. The L-value range of the WD spectrometer used is 55 mm ≤ L ≤ 255 mm. Thus, the detectable energy with the PET crystal ranges from 1550 eV to 7200 eV according to equation (1).

$$E = \frac{12398 \cdot R}{d \cdot L} \tag{1}$$

The numerical equation (1) was derived from Bragg's law and the Rowland circle conditions for the WD spectrometer used. Here, E [eV] is the radiation energy, L [mm] is the L value, R [mm] is the diameter of the Rowland circle, and d [Å] is the periodicity of the dispersing element. For the spectrometer used, the diameter of the Rowland circle is 140 mm.

The energy of the exciting electrons, E_0, was set to 20 keV in all measurements. The probe current used was, depending on the sample and the reflecting order, in the range between 10 nA and 1 µA. In order to reduce the sample strain, the probe diameter was widened to 100 µm. The effect of beam widening concerning potential spectra deterioration was carefully proofed previously by a series of measurements with different probe diameters. Here, spectral changes are vanishing for probe diameters below 200 µm.

If the PET crystal is used, the X-rays in our microprobe are detected by a sealed Xe-filled proportional counter (XPC). Nearly all WDS spectra were recorded in the differential pulse height analysis mode. But in order to determine optimized measuring conditions, spectra were initially recorded in the integral mode. The XPC voltage and the gain of the pulse amplifier were selected in such a manner that the mean pulse height of the detected X-ray quanta was 4 V.

As standard samples we have selected the three elements potassium (^{19}K), cadmium (^{48}Cd), and uranium (^{92}U), which exhibit intensive (K, L, M)$\alpha_{1,2}$-doublets of nearly comparable energy. The relevant line energies, taken from the compilation tabulated by Bearden [9], are summarized in Table 1.

With the exception of potassium, pure element metal standards were used. Nearly all metals have a more or less strong tendency to oxidize. By grinding the samples immediately before the measurement, we were able to strongly reduce the ^{8}O Kα-intensity to a negligible level. For the potassium measurements a polished KBr sample was used. This sample was, in order to avoid charging effects, coated with approximately 20 nm of carbon.

Table 1. $\alpha_{1,2}$-line energies for the K-radiation of K, the L-radiation of Cd, and the M-radiation of U (values are rounded to full eV; data taken from [9]).

Transition/Line	^{19}Potassium	^{48}Cadmium	^{92}Uranium
KL_3 (α_1)	3314 eV	-	-
KL_2 (α_2)	3311 eV	-	-
L_3M_5 (α_1)	-	3134 eV	-
L_3M_4 (α_2)	-	3127 eV	-
M_5N_7 (α_1)	-	-	3171 eV
M_5N_6 (α_2)	-	-	3160 eV

3. Results and discussion

3.1. Resolution enhancement

In figure 1 the energy difference $\Delta E = E(\alpha_1) - E(\alpha_2)$ for K-, L-, and M-radiation versus the atomic number Z is shown. In the classic compilation by Bearden [9], separated energies for α_1- and α_2-lines are listed first for Z > 12 (K-radiation), Z > 36 (L-radiation), and Z > 73 (M-radiation). As illustrated in figure 1, ΔE rises rapidly with increasing Z. The elements used in this work are marked by dotted lines. Here, the energy difference ranges from 3 eV for potassium up to 11 eV in the case of uranium.

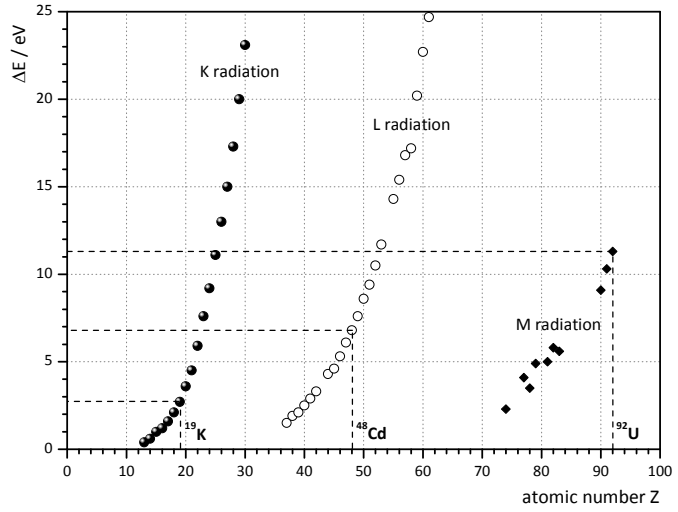

Figure 1. Energy difference $\Delta E = E(\alpha_1) - E(\alpha_2)$ versus atomic number Z. ΔE rises rapidly with increasing Z. The line energies were taken from reference [9].

In none of these cases were we able to resolve the (K, L, M)$\alpha_{1,2}$-doublets into their components when recording X-ray spectra in first order reflection with our setup. The resolving power of a given WD spectrometer is mainly determined by the crystallographic perfection of the dispersing element used. Furthermore, a high dispersion, $D = \Delta\theta/\Delta\lambda$, of this element is crucial for sufficient line separation. More details in this regard can be found e.g., in the monograph written by Reed [4].

Nevertheless, using a given setup, it is possible to enhance the spectrometer resolution significantly. For instance, one can narrow the entrance slit of the detector in order to exclude reflections originating from the parts of the crystal which are outside of the Rowland circle plane. Another, more powerful way involves the use of the nonlinear resolving power of Johannson-type

WD spectrometers. In order to illustrate this point initially, one has to consider the spectrometer position of the radiation of interest. The energy of the (K, L, M)$\alpha_{1,2}$-line doublets of the three elements used in this work is comparable in the range slightly above 3 keV. According to figure 2, the spectrometer position of the radiation of this energy is – using our spectrometer setup – between 120 mm ≤ L ≤ 125 mm.

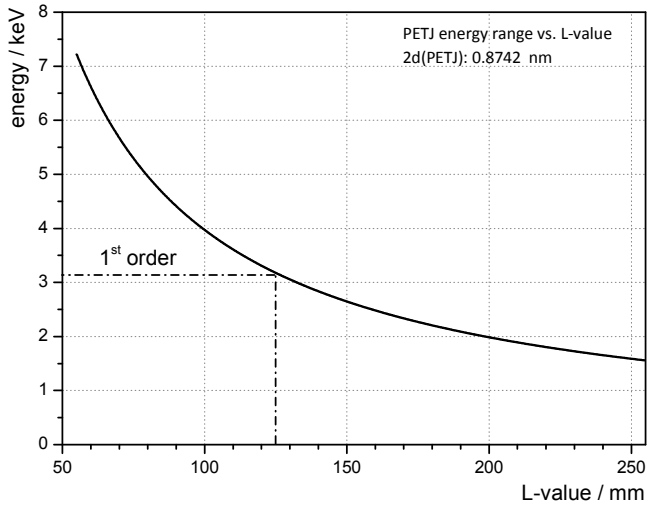

Figure 2. Dependency of the detectable energy range versus the spectrometer position. The curve was calculated using equation 1. The approximate spectrometer position of the lines of interest in first order reflection is marked.

By recording the X-ray spectra in second order reflection, they will be transferred to twice the initial L value of the first order into a region in which X-ray quanta of half the energy are normally detected. This means that we will find the second order reflection of the three line doublets between 240 mm ≤ L ≤ 250 mm. In order to better understand the advantageous consequences of this, one has to differentiate Eq. 1.

$$\frac{\Delta E}{\Delta L} = f(L) = \frac{-397099}{L^2} \tag{2}$$

In this manner, one is able to calculate the energy difference, ΔE, for one fixed increment, ΔL. In figure 3, this has been done for a typical interval of ΔL = 100 µm.

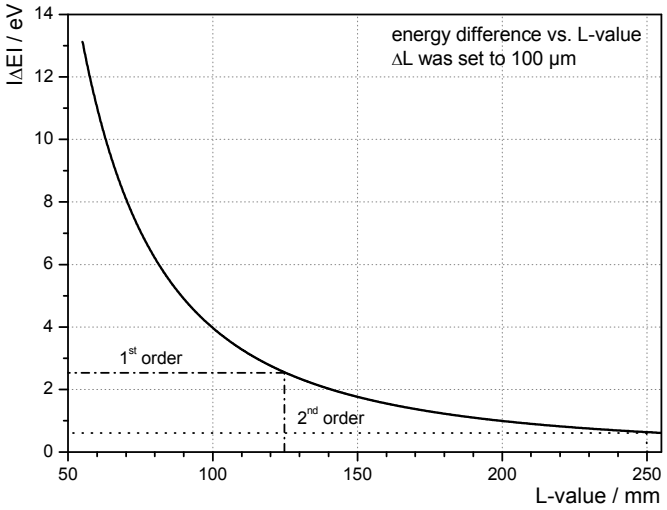

Figure 3. Dependency of the energy difference, ΔE, from the spectrometer position, calculated for a fixed interval of ΔL = 100 µm. The lines of interest in first (dashed-dotted) and second order (dotted) reflection are marked.

The curve shown in figure 3 makes it clear that the theoretical energy resolution of the lines of interest in the frame of the measurement conditions in first order reflection cannot be better than nearly 3 eV. In contrast, by changing to second order spectrometry and thus shifting the spectra towards larger L-values, the resolution limitation can be lowered to approximately 0.5 eV. Consequently, in second order reflection a given X-ray spectrum extends a much larger L-value range than in first order reflection and the line separation is greatly improved. In practice, the measured energy resolution is – as already mentioned – determined by several additional aspects. It is generally much worse than the theoretical considerations. One option for an experimental approach to estimating the real spectrometer resolution as a function of the L-value is to measure one and the same element in first, second, and third order reflection. Then, one can determine the full width at half maximum (FWHM) of a given X-ray line as a measure of the resolving power. Suitable lines for this purpose are K-lines initially because they are narrower than both L-lines and M-lines. Figure 4 shows the natural KL_3 (α_1)-line widths (FWHM) of the elements $10 \leq Z \leq 30$. These values were taken from reference [10].

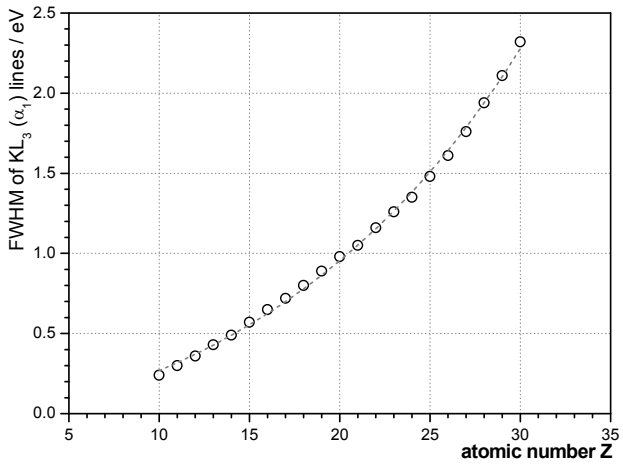

Figure 4. Natural KL_3 (α_1)-line width (FWHM) for the elements $10 \leq Z \leq 30$. The data were taken from Krause *et al* [10].

One element usually used to specify the resolving power of energy-dispersive X-ray spectrometers is ^{25}Mn. Mn is also suitable for the specification of a WD spectrometer. The energy of Mn-Kα_1 is 5899 eV, and that of Kα_2 is 5888 eV. Using the PET crystal our spectrometer is able to detect the Mn $KL_{2,3}$ ($\alpha_{1,2}$)-radiation in first, second, and third order reflection. In this connection, it is assumed that the actual spectrometer resolution is always worse than the natural ^{25}Mn $KL_{2,3}$ ($\alpha_{1,2}$)-line width. Figure 5 shows the experimentally estimated FWHM values for the three reflection orders versus the L-value.

The natural line widths of the ^{25}Mn K-lines were given by Krause to 1.48 eV and 1.50 eV, respectively. The energy difference, $\Delta E = E(\alpha_1) - E(\alpha_2)$, is about 11 eV, and the relative line intensity, α_2/α_1, is shown in White and Johnson [11] to be about 50 %. Consequently, the overall FWHM of the unresolved K$\alpha_{1,2}$-line is expected to be significantly broader than the values for each single line.

In first and second order reflections we were unable to resolve the ^{25}Mn K$\alpha_{1,2}$-doublet. Here, we have estimated the FWHM to 75 eV in the first order and to 10 eV in the second order. In third order reflection we were able to separate the Kα_1- and Kα_2-line; thus, we have estimated the Kα_1 FWHM to be approximately 3 eV. Here, one can directly compare the measured and the "true" line width and thus estimate the resolving power at that spectrometer position. For the first and second order measurement, the uncertainty is greater because of the unknown line width. Nevertheless, the second order measurement, in which the Mn K$\alpha_{1,2}$-doublet is still unresolved, indicates an overall FWHM of

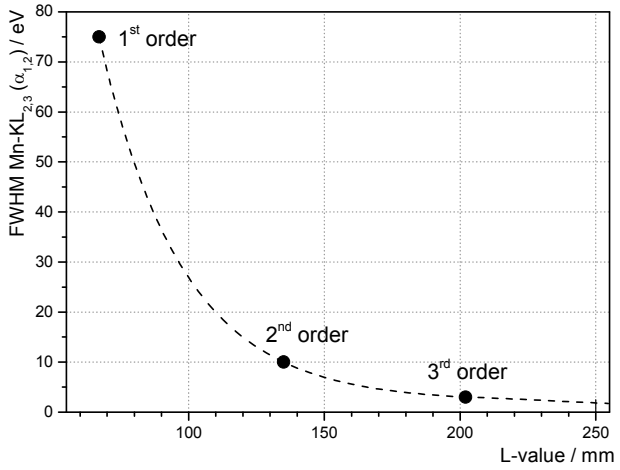

Figure 5. Measured ^{25}Mn $KL_{2,3}$ ($\alpha_{1,2}$)-line widths (FWHM) in first and second order reflection. In the third order, the $\alpha_{1,2}$-doublet is resolved, and therefore, only the α_1 FWHM is shown.

no more than 10 eV and this value seems to be mainly determined by the energy difference $\Delta E = E(\alpha_1) - E(\alpha_2)$

3.2. Discriminator settings

By changing from first to second order spectrometry, the lines are transferred to twice of the initial spectrometer position. Here, normally X-ray quanta of half the energy are detected. In the case of our standard measurements this concerns solely continuous bremsstrahlung and consequently the second order spectrum involves now bremsstrahlung reflected in both the first and the second order. This fact leads to a worsening of the peak-to-background ratio.

In order to enhance the detection capability of the second order lines, the counter settings must be optimized quite carefully. For this purpose, we initially choose a sufficient gain according to the energy of the detected X-ray quanta. Then, a so called high-voltage scan was performed to determine the optimal detector high voltage. Thereby, a lower gain requires a higher voltage and consequently a higher gain a lower voltage to achieve one and the same pulse height of the detected X-ray quanta. An optimal combination of gain and high voltage for a given X-ray quantum energy leads in our microprobe always to a mean pulse height of 4 V. A corresponding base level scan is shown in figure 6. Here, the base line is set to 3 V, and the window width amounts to 2 V. Consequently, only pulse energies within this window will contribute to the differential mode measurement.

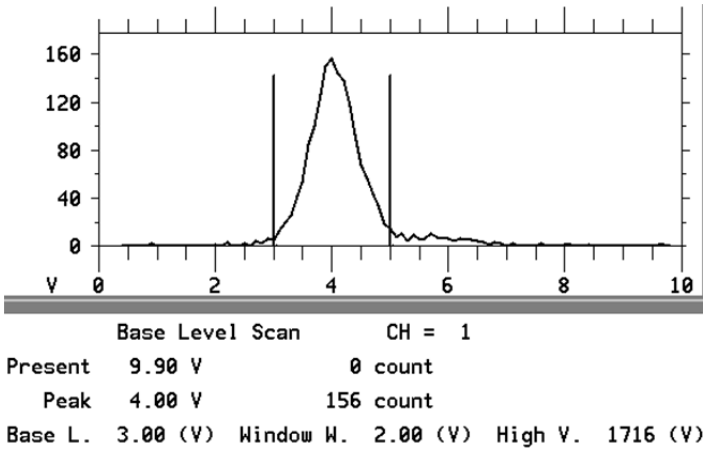

Figure 6. Base level scan for second order ^{19}K KL_3 (α_1)-quanta. The gain and the high voltage of the XPC were selected so that the mean pulse height was 4 V.

In order to determine the optimized discriminator settings in the first step, we used the so-called integral detection mode. In this step, a base line is set and all pulses above this base line contribute to the measured X-ray spectrum. In our experiments we started at a low base level of 1 V. Consequently, the resulting (K, L, M)$\alpha_{1,2}$ second order spectrum exhibited a poor peak-to-background (P/B) ratio because a broad bremsstrahlung spectrum (reflected in both the first and second order) contributes to the measurement. Then, we increased the base level step by step and recorded X-ray spectra after each single step. By doing so, we excluded radiative contributions step by step starting at the low energy side of the incoming spectral range. This applies in particular to background radiation of half the energy detected in first order reflection.

As a measure of optimisation, the product of P/B times net peak intensity (PBNP) was used. The dependency of this value as a function of the base level setting is shown for the potassium KL_3 (α_1)-radiation in figure 7a. In addition, figure 7b shows the corresponding detection limit (DL) for ^{19}K KL_3 (α_1)-radiation in potassium bromide (KBr).

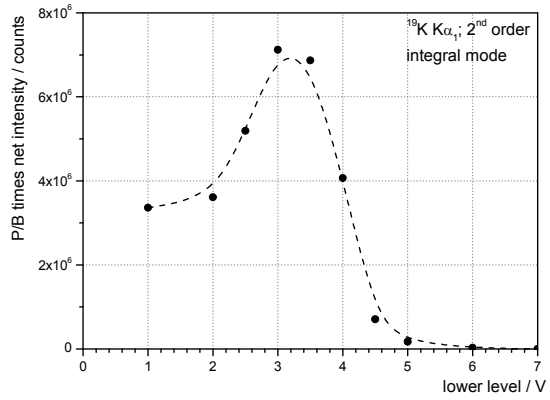

Figure 7a. P/B times net peak intensity (PBNP) versus the base level setting. The chart exhibits a maximum at a lower level of 3 V.

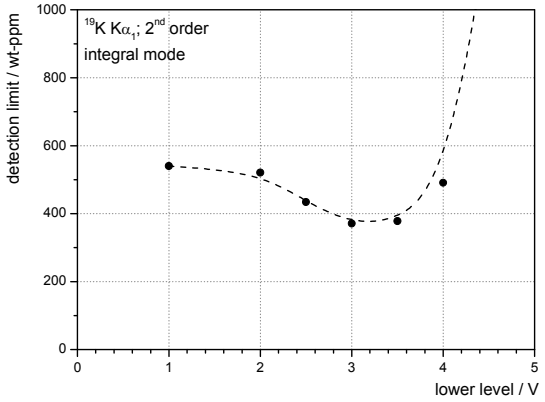

Figure 7b. Corresponding detection limit of K-Kα_1 in KBr. Also here, an optimized setting around 3 V can be observed.

The detection limits for each single step and for each single spectrum were estimated using equation 3.

$$DL = 3 \cdot \sqrt{BG} \tag{3}$$

Here, BG is the background intensity [counts], and DL is the calculated detection limit [counts] which is then converted into a concentration. To do this, the K-Kα_1 net intensity is measured in relation to it and normalized concerning the KBr stoichiometry. Both the PBNP chart and the DL curve indicate an optimum lower level around 3 V. By further increasing the base level, a progressive discrimination of the actual peak signal is carried out. Consequently, the PBNP course drops, whereas the detection capability gets worse and worse.

In the second step of optimisation, the base level was set to the ascertained value of 3 V as done in the first experimental step. Then, the window width was reduced step by step, and again here spectra were recorded after each step. This strategy leads to a step-by-step suppression of the high energy spectral part of the incoming radiation. The subsequent effect is expected to be much smaller than the base level adaption implemented in step one because the high energy contributions belong mainly to the second order spectrum. The results of this series of measurements are shown in figure 8a. At a

decrease in window width, an increasing tendency can be observed in the PBNP value. This behaviour can mainly be explained by a lowering of the background intensity and thus an enhancement of the P/B ratio. When the window width becomes even narrower than 1.5 V, the PBNP value drops immediately due to the progressive discrimination of the actual peak signal. Here, too, detection limits were estimated for the K $K\alpha_1$-radiation in the KBr compound. The course of the curve mirrors inversely those of the PBNP value as shown in figure 8b.

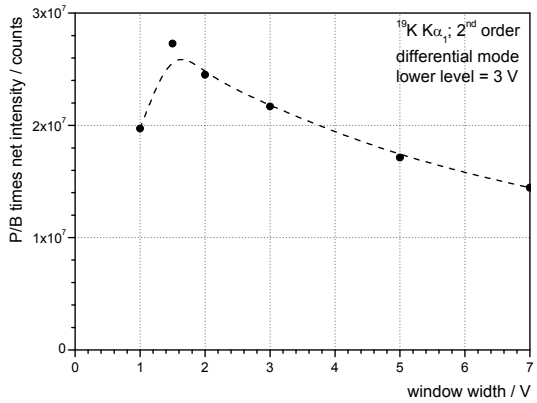

Figure 8a. P/B times net peak intensity (PBNP) versus window width. The course exhibits a maximum at 1.5 V.

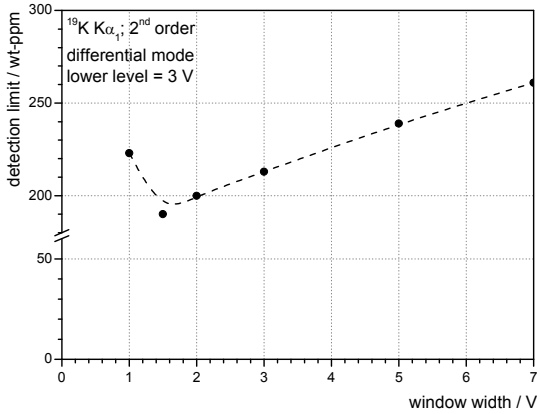

Figure 8b. Corresponding detection limit for K-$K\alpha_1$ in KBr. Again, the best detection capability is achieved at a window width of 1.5 V.

3.3. Measurements

The $KL_{2,3}$ $(\alpha)_{1,2}$-lines of ^{19}K, the $L_3M_{4,5}$ $(\alpha)_{1,2}$-lines of ^{48}Cd, and the $M_5N_{6,7}$ $(\alpha)_{1,2}$-lines of ^{92}U recorded in first (a) and second (b) order reflection are shown in figures 9, 10, and 11. The second order measurements were carried out using the optimized discriminator setting procedure described in section 3.2.

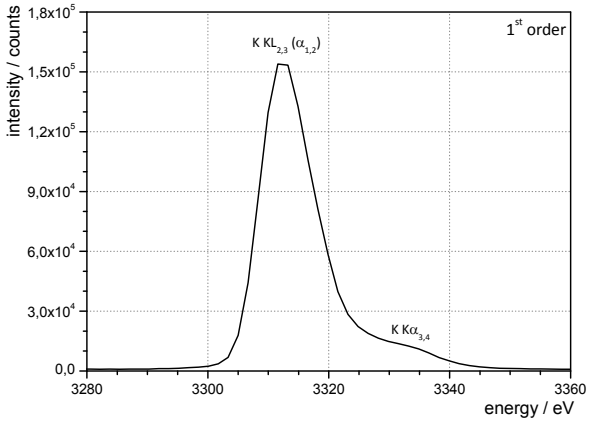

Figure 9a. Unresolved $KL_{2,3}$ $(\alpha)_{1,2}$-lines of ^{19}K recorded in first order reflection. On the high energy side of $K\alpha_{1,2}$ the weak satellite line $K\alpha_{3,4}$ is observable.

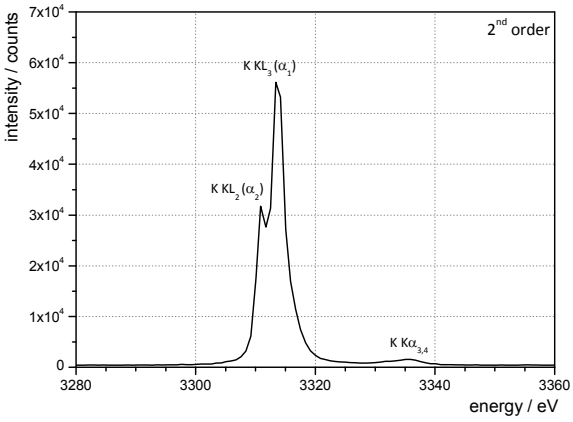

Figure 9b. $KL_{2,3}$ $(\alpha)_{1,2}$-lines of ^{19}K recorded in second order reflection. Here, the $K\alpha_2$ line can be clearly observed.

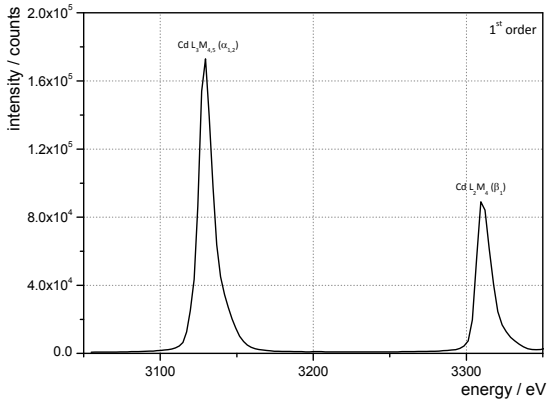

Figure 10a. Unresolved $L_3M_{4,5}$ $(\alpha)_{1,2}$-lines and L_2M_4 (β) of ^{48}Cd recorded in first order reflection.

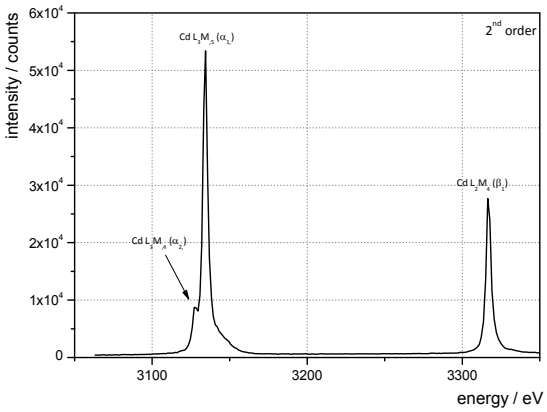

Figure 10b. ^{48}Cd L-lines recorded in second order reflection. Here, the L_3M_4 (α_2) -line can be clearly observed.

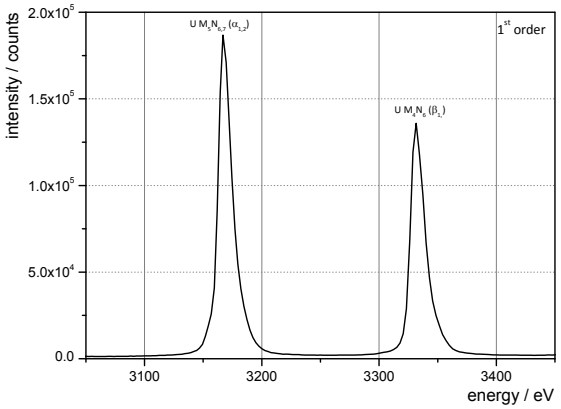

Figure 11a. Unresolved $M_5N_{6,7}$ $(\alpha)_{1,2}$-lines and M_4N_6 (β) of ^{92}U recorded in first order reflection.

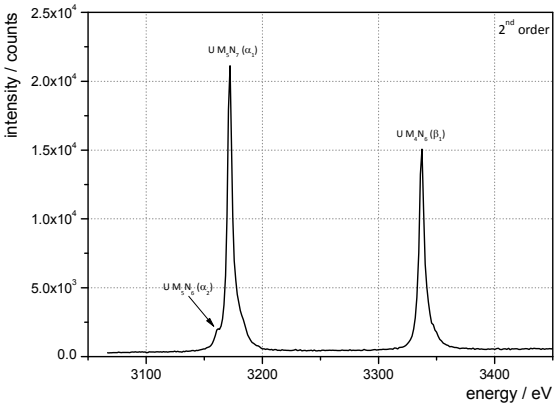

Figure 11b. ^{92}U M-lines recorded in second order reflection. Here, the M_5N_6 (α_2)-line is visible as a low energy shoulder of M_5N_7 (α_1).

In the case of the second order measurements, we were able to resolve the (K, L ,M)$\alpha_{1,2}$-doublets of all three elements into their components α_1 and α_2. This enabled us to estimate α_2/α_1 intensity ratios and to compare these values with the established literature. Furthermore, we estimated FWHM data for the unresolved $\alpha_{1,2}$-doublets in the case of the first order measurements and for the separated α_1-line in the case of the second order measurements. All results are summarized in Table 2.

The FWHM data compiled in Table 2 show the resolution enhancement connected with the transition from first to second order spectrometry. By shifting the spectrometer position to twice the first order L value, we observed a FWHM decrease by a factor of approximately 3. The estimated FWHM values agree for potassium and cadmium qualitatively well with the spectrometer performance curve shown for Mn K-radiation in figure 5. For these two elements as well as the manganese, the natural line widths are in a comparable range. Some data available in the literature are shown in Table 3. Due to the lack of reliable data for Cd L-lines, we have used those of the neighbouring element silver.

Table 2. $\alpha_{1,2}$-spectrometer position for first and second order, line widths (FWHM) and relative intensities for the K-radiation of K, the L-radiation of Cd, and the M-radiation of U.

X-ray line	Order	L value [mm][a]	FWHM [a,b] [eV]	α_2/α_1 intensity ratio [%]	
				Present work	Other literature[c]
K-$KL_{2,3}$ ($\alpha_{1,2}$)	1	120	10	-	
K-$KL_{2,3}$ ($\alpha_{1,2}$)	2	240	3	50	50
Cd-$L_3M_{4,5}$ ($\alpha_{1,2}$)	1	127	10	-	
Cd-$L_3M_{4,5}$ ($\alpha_{1,2}$)	2	254	3	10	10
U-$M_5N_{6,7}$ ($\alpha_{1,2}$)	1	125	14	-	
U-$M_5N_{6,7}$ ($\alpha_{1,2}$)	2	250	6	5	100!

[a] For second order spectra, the α_1-data are shown; [b] values are rounded to full eV; [c] relative intensities shown in [11].

Table 3. Natural line widths for selected K- and L-lines found in the literature.

Element/line	Natural line width [eV]	Reference
K-KL_3 (α_1)	0.89	[10]
K-KL_2 (α_2)	0.89	[10]
Mn-KL_3 (α_1)	1.48	[10]
Mn-KL_2 (α_2)	1.50	[10]
[a]Ag-L_3M_5 (α_1)	2.34	[12]
[a]Ag-L_3M_4 (α_2)	2.20	[12]
U-M_5N_7 (α_1)	-	-
U-M_5N_6 (α_2)	3.40	[13]

[a] Instead of the Cd L-line widths, those of the neighbouring element silver are shown.

In the case of K and Cd we can conclude that the spectrometer resolution limits the measured FWHM values because the natural line widths are significantly smaller. It has to be said that in the case of the first order spectrum of potassium, the relatively intensive KL_2 (α_2)-line contributes to the line width of the unresolved doublet; therefore, it is expected to be somewhat broader than the single α_1-line. Because of the low relative intensity of $L\alpha_2$ and, in particular, $M\alpha_2$ the influence of these lines on the FWHM of the unresolved $\alpha_{1,2}$-doublets can be neglected.

In the case of U M-lines we have determined slightly broader FWHM values, which can mainly be explained by the generally broader line width of M-lines. Unfortunately, we were unable to find a reliable line width for the U M_5N_7 (α_1)-line in the literature. If one uses the energetic spread of the participating subshells as shown in [13], one can estimate the FWHM for U-$M\alpha_1$ to be also approximately 3.5 eV. For U M_5N_6 (α_2) a FWHM value of 3.4 eV is shown in the same reference.

Through the evaluation of the second order spectra we have estimated α_2/α_1 intensity ratios which are also shown in Table 2. However, according to the close energy proximity the determination of the α_2 net intensity can only be a rough approximation. Nevertheless, our values for potassium and

cadmium correspond well with literature references. In contrast, a great discrepancy was observed in the case of uranium. We reported in a previous work about the possible causes of this [8]. A rough prediction of relative intensities of characteristic X-ray lines can be made applying the Burger-Dorgelo rule (Burger and Dorgelo, 1924). This approximation leads to α_2/α_1 intensity ratios of 50 % for ^{19}K, 11 % for ^{48}Cd, and 5 % for ^{92}U, which corresponds well with our experimental results. A short but instructive example of such a calculation was presented in Reed (p. 300) in his monograph [4].

4. Concluding remarks

The resolving power of a given wavelength-dispersive X-ray spectrometer exhibits a strong L-value dependency. If an X-ray line is detectable in first and second order reflection as well, one can reach a significantly improved energy resolution by choosing the second order. It was possible in this manner only to resolve the (K, L, M)$\alpha_{1,2}$-doublets of the elements potassium, cadmium, and uranium into their components and to estimate α_2/α_1 intensity ratios. Except for the M$\alpha_{1,2}$-radiation of uranium, our α_2/α_1-intensity values correspond well with the data shown in the literature.

A significant loss of intensity is connected with the transition to the second order reflection, which can, at least partially, be compensated by increasing the probe current. In addition, the background intensity is increased because the bremsstrahlung reflected in first as well as in second order reflection contributes to the measurement. Therefore, it is of great importance to optimize the discriminator settings in order to maintain sufficient peak-to-background ratios and, consequently, sufficient detection limits. By doing so, we were able to reach nearly the same detection limit for ^{19}K Kα_1-radiation in KBr in the second order spectra as in first order reflection. Consequently, it can be concluded that the strategy of second order spectrometry can be a helpful performance gain for the solution of tricky analytical tasks.

References

[1] Kirchhof J, Unger S, Dellith J, Scheffel A and Teichmann C 2012 Diffusion coefficients of boron in vitreous silica at high temperatures. *Optical Materials Express* **2** 534
[2] Müller R 1967 *Spektrochemische Analysen mit Röntgenfluoreszenz*. (Munich & Vienna: R. Oldenburg Verlag)
[3] Jenkins R 1977 *An introduction to X-ray spectrometry*. (Heyden & Son; ISBN 0-85501-035-5)
[4] Reed S J B 1993 *Electron probe microanalysis, 2nd edition*. (Cambridge: Cambridge University Press; ISBN 0-521-41956-5)
[5] Scott V D, Love G and Reed S J B 1995 *Quantitative electron probe microanalysis, 2nd edition*. (Ellis Horwood; ISBN 0-13-104050-2)
[6] Goldstein J *et al* 2003 *Scanning electron microscopy and X-ray microanalysis, 3rd edition*. (Springer Verlag; ISBN 0-306-47292-9)
[7] Dellith J and Wendt M 2007 The M emission spectrum of 68erbium. *Microsc. Microanal.* **13** 191-195
[8] Dellith J, Scheffel A, Terborg R and Wendt M 2011 Reinvestigation of the M emission spectrum of 92uranium. *Microsc. Microanal.* **17** 296-301
[9] Bearden J A 1967 X-ray wavelengths. *Rev. Mod. Phys.* **39** 78-124
[10] Krause M O *et al* 1979 Natural line widths of atomic K- and L-levels, Kα X-ray lines and several KLL Auger lines. *J. Phys. Chem. Ref. Data* **8** no. 2
[11] White E W and Johnson G G 1970 Emission and absorption wavelengths and two-theta tables. *ASTM Data Series DS37A*. (Philadelphia)
[12] Parratt L G 1938 The silver L series X-ray spectrum: line widths, wavelengths, relative intensities, satellites, and widths of energy levels. *Phys. Rev.* **54** 99-114
[13] Zschornack G 2007 *Handbook of X-ray data*. (Springer Verlag; ISBN 978-3-540-28618-9)